Engineered Nanostructures of Haptens Lead to Unexpected Formation of Membrane Nanotubes Connecting Rat Basophilic Leukemia Cells

Jie-Ren Li,[†] Shailise S. Ross,[†] Yang Liu,[†] Ying X. Liu,[†] Kang-hsin Wang,[†] Huan-Yuan Chen,[‡,§] Fu-Tong Liu,[‡,§] Ted A. Laurence,[∥] and Gang-yu Liu*[,†]

[†]Department of Chemistry, University of California, Davis, California 95616, United States, [‡]Department of Dermatology, School of Medicine, University of California, Davis, Sacramento, California 95817, United States, [§]Institute of Biomedical Sciences, Academia Sinica, Taipei, Taiwan, ROC, and [∥]Lawrence Livermore National Laboratory, Livermore, California 94550, United States

ABSTRACT A recent finding reports that co-stimulation of the high-affinity immunoglobulin E (IgE) receptor (FcεRI) and the chemokine receptor 1 (CCR1) triggered formation of membrane nanotubes among bone-marrow-derived mast cells. The co-stimulation was attained using corresponding ligands: IgE binding antigen and macrophage inflammatory protein 1α (MIP1 α), respectively. However, this approach failed to trigger formation of nanotubes among rat basophilic leukemia (RBL) cells due to the lack of CCR1 on the cell surface (*Int. Immunol.* 2010, *22* (2), 113−128). RBL cells are frequently used as a model for mast cells and are best known for antibody-mediated activation *via* FcεRI. This work reports the successful formation of membrane nanotubes among RBLs using only one stimulus, a hapten of 2,4-dinitrophenyl (DNP) molecules, which are presented as nanostructures with our designed spatial arrangements. This observation underlines the significance of the local presentation of ligands in the context of impacting the cellular signaling cascades. In the case of RBL, certain DNP nanostructures suppress antigen-induced degranulation and facilitate the rearrangement of the cytoskeleton to form nanotubes. These results demonstrate an important scientific concept; engineered nanostructures enable cellular signaling cascades, where current technologies encounter great difficulties. More importantly, nanotechnology offers a new platform to selectively activate and/or inhibit desired cellular signaling cascades.

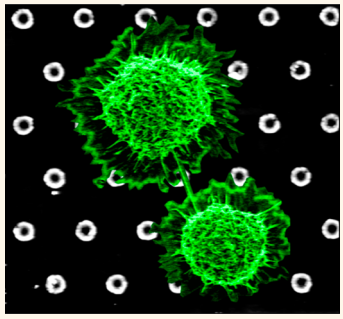

KEYWORDS: membrane nanotubes · rat basophilic leukemia (RBL) cells · mast cells · atomic force microscopy (AFM) · scanning electron microscopy (SEM) · haptens · particle lithography

Membrane nanotubes provide membrane continuity among connected cells and enable intercellular exchange of both membrane-carrying molecules and cytoplasmatic content.[1,2] The communication *via* membrane nanotubes plays an important role in many physiological processes including immune defense,[3,4] tumorigenesis,[2,5−7] transmission of pathogens,[8,9] and cell differentiation.[10,11] Membrane nanotubes have been observed in many cell types, including neuronal cells such as the neuron-like pheochromocytoma cell line (PC12)[12] and immune cells such as NK cells,[13] dendritic cells,[3] macrophages,[14] and T cells.[9]

Our team has been investigating immune processes involving mast cells,[15−17] which are best known for their antigen-induced activation and involvement in immediate-type hypersensitivity.[17−29] Mediators released upon activation can initiate immediate vascular responses and modulate acquired- and innate-immune reactions.[18,30−32] Prior studies have also shown that cytoneme-like nanotubes could form among bone-marrow-derived mast cells (BMMCs).[33] Unlike antibody-mediated activation, which requires clustering or stimulation of the high-affinity immunoglobulin E (IgE) receptor (FcεRI), receptors mediated by IgE nanotube formation are triggered by the co-stimulation of FcεRI and chemokine receptor (CCR1) by antigen and ligand, such as human serum albumin containing 2,4-dinitrophenyl (DNP-HSA) and macrophage inflammatory protein 1α (MIP-1α), respectively. Within 5 min of co-stimulation, nanotubes would appear that link the nearest neighboring cells to enable long-distance intercellular communication.[1,18,33]

* Address correspondence to gyliu@ucdavis.edu.

Received for review April 16, 2015 and accepted June 9, 2015.

Published online June 09, 2015
10.1021/acsnano.5b02270

In contrast to BMMCs, rat basophilic leukemia (RBL-2H3) cells, another frequently used model for mast cells, do not form cytoneme-like structures using the co-stimulations approach.[33] The lack of the chemokine receptor CCR1 on the surface of RBLs was inferred as the cause. Even after being transfected with CCR1, anti-DNP IgE-sensitized RBL cells form cytoneme-like structures only in low frequency after co-stimulation of DNP-HSA and MIP-1α.[33]

Our prior work demonstrated that nanotechnology offers a new means to present antigens and to impact cellular signaling cascades.[16] For example, arrays of nanogrids of antigen could activate mast cells to a higher degree than using soluble forms of antigen.[16] Using RBL cells, this work investigates if nanotechnology could facilitate cellular signaling cascades that are otherwise extremely difficult to activate, *e.g.*, formation of membrane nanotubes. Our results indicate that arrays of nanorings lead to the formation of membrane nanotubes among RBL cells. The length and prevalence of membrane nanotubes appear to vary with the spatial distribution of hapten nanostructures.

It is known that mast cells vary widely in their responses to stimuli, mediator content, differentiation status, and receptor expression.[18] It is inferred that mast cells could utilize a variety of pathways and mechanisms to regulate immune responses.[33] The enabling of membrane nanotube formation among mast cells using nanotechnology offers a new platform to impact and to perhaps regulate mast-cell-based immune processes. These results demonstrate an important scientific concept: engineered nanostructures enable cellular signaling cascades, where current technologies encounter great difficulty. More importantly, nanotechnology provides a new and very promising approach to selectively activate desired cellular signaling cascades.

RESULTS AND DISCUSSION

Presenting Haptens Using Nanolithography. We utilized particle lithography combined with surface chemistry to attach 2,4-dinitrophenyl (DNP) to silicon surfaces. The geometry of the individual features and the periodicity of nanostructures are dictated by the packing and the diameter of template particles. The step-by-step protocol is detailed in the Methods section. Six polystyrene microspheres were used as templates with diameters of 1000, 800, 500, 300, 240, and 200 nm, respectively. The resulting DNP nanostructures were referred to as Nano1, Nano2, Nano3, Nano4, Nano5, and Nano6, respectively. All six DNP nanostructures were characterized using atomic force microscopy (AFM). Figure 1 shows the topographic images of representative nanostructures from each category. In Nano2, as shown in Figure 1A, each DNP feature is presented as a nanoring. The height of a typical ring measures 1.2 nm above the surroundings and 119 nm wide (full width at half-maximum, FWHF, in topographs). The inner ring diameter is 148 nm, with the center-to-center distance of 802 nm. Among tens of nanorings measured from AFM images, the periodicity (center-to-center distance), inner ring diameter, width, and height of the ring frame are measured and summarized in Table 1. The array of DNP rings covered the entire silicon surface (1 × 1 cm^2). The surface DNP coverage in Nano2 is 20 ± 1%. The individual features for all six nanostructures are rings of varying geometry. The feature size, geometry, and periodicity for Nano1−Nano6 were also characterized using AFM, as shown if Figure 1 and summarized in Table 1. From Nano1 to Nano6, periodicities decrease from 1001 ± 11 nm to 207 ± 6 nm, while the DNP coverage increases from 15% to 72%.

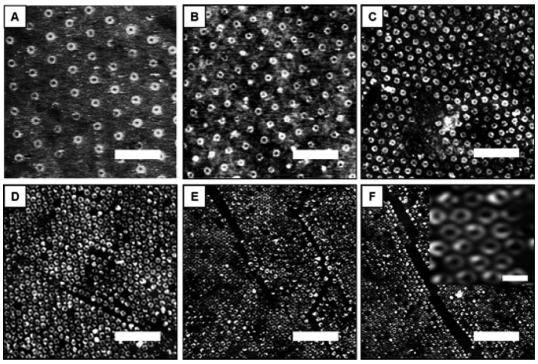

Figure 1. AFM topographs of six DNP nanostructures: (A) Nano1, (B) Nano2, (C) Nano3, (D) Nano4, (E) Nano5, and (F) Nano6. Inset in (D) shows a zoom-in view. Scale bars are 2 μm and 200 nm for images and inset, respectively. All AFM images were acquired under contact mode in ambient condition, with imaging force ranging from 15 to 25 nN.

Hapten Nanostructures Lead to Membrane Nanotube Formation among RBL-2H3 Cells. Upon sensitizing RBL cells with anti-DNP IgE, the cell morphology was monitored after exposure to Nano2 for 1 h. Membrane nanotubes appeared, as shown in Figure 2A: 6.75 μm long with a diameter of 76 nm. The zoom-in views (Figure 2B1 and B2) clearly reveal that the origins of the membrane nanotube were above the contact plane of the substratum. This observation is consistent with the previously seen membrane nanotubes among PC12 cells.[12] The above criteria are important to distinguish membrane nanotubes from filopodia. The PC12 membrane nanotubes, also characterized by SEM, measured in diameter from 50 to 200 nm and in length ranging from 10 to 150 μm. The RBL membrane nanotubes are of a similar diameter, but shorter in length than those among PC12 cells. In a typical SEM scan (400 × 300 $μm^2$), over 70 RBL cells were visible; among them, nine cells were involved in membrane nanotube formation, yielding a prevalence of 12.5%. From four sets of experiments, containing over 1000 RBL cells, the prevalence of membrane nanotubes was found to be 12 ± 3%.

TABLE 1. Structural Characterization of DNP Nanostructures from AFM Topographs

	ring width (nm)	inner diameter of ring (nm)	apparent height (nm)	periodicity (nm)	DNP coverage (%)
Nano1	137 ± 9	169 ± 7	1.1 ± 0.3	1001 ± 11	15 ± 1
Nano2	127 ± 7	153 ± 6	1.2 ± 0.3	807 ± 10	20 ± 1
Nano3	107 ± 7	117 ± 5	1.3 ± 0.3	507 ± 9	34 ± 2
Nano4	77 ± 8	92 ± 4	1.1 ± 0.4	305 ± 7	51 ± 3
Nano5	67 ± 8	81 ± 5	1.2 ± 0.3	241 ± 6	62 ± 5
Nano6	63 ± 7	71 ± 4	1.2 ± 0.4	207 ± 6	72 ± 6

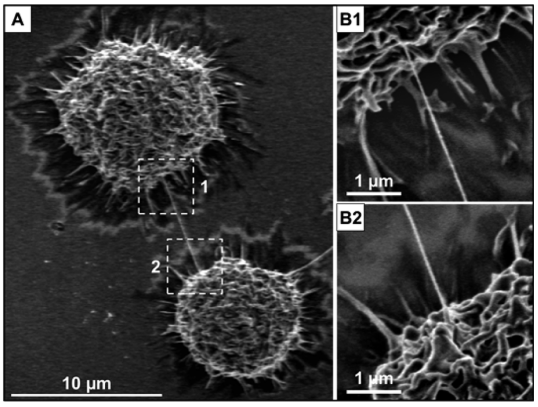

Figure 2. (A) SEM image of two RBL cells connected by a membrane nanotube. (B1) Zoom-in view of frame 1 indicated in (A). (B2) Zoom-in view of frame 2 indicated in (A).

In addition to the most commonly known situation, a single membrane nanotube bridging two neighboring cells, a single cell forming multiple nanotubes was also observed, as shown in Figure 3. In Figure 3A, five RBL cells were sequentially connected with four membrane nanotubes, forming an RBL "necklace". In Figure 3B, one RBL cell in the center formed multiple intercellular membrane nanotubes connected with three surrounding cells. Two of the RBL cells were connected to the center cell by single nanotubes. The third cell is connected by two membrane nanotubes with the center RBL cell. These intercellular membrane nanotube networks were also observed among other cell lines, such as PC12,[12] human lung carcinoma A549 cells,[34] and rat cardiac myoblast (H9c2) cells.[35] Our observations represent the first found in RBL-2H3 cells. These complex networks of membrane nanotubes could provide a structural base for intercellular communication and transport among RBL cells.[2,36] In addition, this outcome suggests a high possibility for mast cell−T cell communication *via* membrane nanotubes.[2,37−39]

Spatial Arrangement of Hapten Nanostructures Impacts Formation of Membrane Nanotubes. When reducing the periodicity of DNP nanorings from Nano1 to Nano6, both the nanotube length and formation prevalence changed accordingly. Typical examples are shown in Figure 4, where the nanotube lengths measure 10, 8.1, 6.2, 5.7, 5.6, and 3.5 μm in the six hapten nanostructures, respectively. Among hundreds of membrane

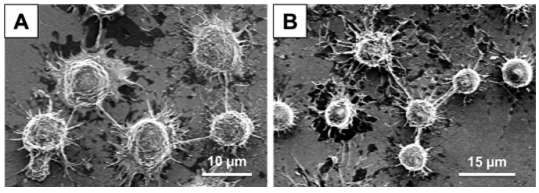

Figure 3. (A) SEM image of five RBL cells connected in series by membrane nanotubes. (B) SEM image of one RBL cell forming multiple membrane nanotubes with neighboring cells.

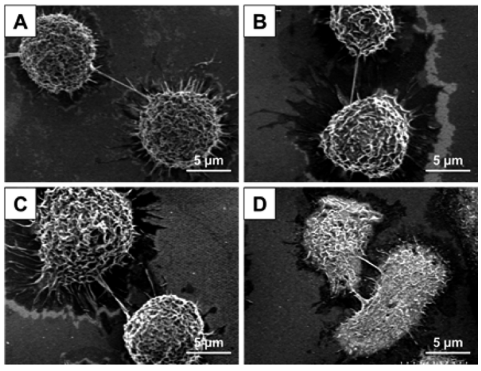

Figure 4. SEM images revealing RBL membrane nanotubes after a 1 h interaction with designated nanostructures of haptens in culture media: (A) Nano2, (B) Nano3, (C) Nano4, and (D) Nano6.

nanotubes measured, the trend of decreasing lengths as a function of the periodicity of the nanorings remains valid, as shown in Figure 5. The length varies within each type of nanostructure, and Figure 5B summarizes all the measurements to reveal the value and deviation. The prevalence of formation of membrane nanotubes increases mildly from 11% to 12% from Nano1 to Nano2, then decreases mildly from 12% to 9% from Nano2 to Nano4, then drops to 5% on Nano5, and finally rapidly drops to below 3% on Nano6, as shown in Figure 5A.

In attempts to rationalize the trends, we measured, as indicated in the previous section and Table 1, the size, periodicity, and coverage of DNP for all nanostructures. To check if the trend is due to the increase in DNP coverage, the nanotube prevalence and length are plotted as a function of DNP coverage, which increases from Nano1 to Nano6 (Figure 5). As a comparison, we investigated RBL cells on self-assembled monolayers (SAMs) with similar DNP coverages. For example,

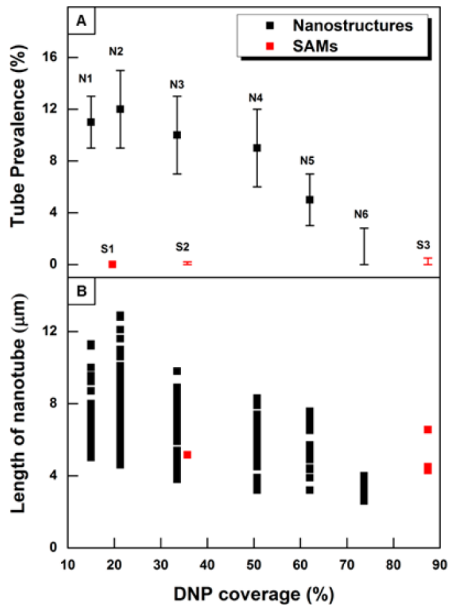

Figure 5. (A) Membrane nanotube prevalence and (B) length are plotted as functions of DNP coverage.

SAM1 has a DNP coverage of 22.6%, similar to that of Nano2 (20%). SAM2 has a DNP coverage of 34.1%, similar to Nano3 (34%), while SAM3 has a DNP coverage of 89.5%, similar to Nano6 (72%). Despite similar coverage, the probability of forming membrane nanotubes in SAMs is much lower than the periodic nanostructures. Upon nanotube formation, the length seems to be similar for SAMs and their nanostructure counterparts. This comparison strongly suggests that local presentations are critical for membrane nanotube formation.

Next, we measured cellular coverage and nearest neighbor cellular separation. From Nano1 to Nano6, cellular coverage increases and the nearest neighbors are located closer. In a typical SEM topograph of 400 × 300 μm^2, the number of cells decreases mildly from 74 to 70, for Nano1 and Nano2, and then increases from 70, 109, 175, 179, and 182 for Nano2, 3, 4, 5, and 6, respectively. The average nearest neighbor cellular separation increases mildly from 39 μm to 42 μm from Nano1 to Nano2 and then decreases from 42, 21, 20, 18, and 10 μm, respectively, from Nano2 to Nano6. In the cases of Nano1−Nano5, the nanotube lengths are much smaller than that of the nearest neighbor separations, also summarized in Table 2. In the case of Nano6, the two cellular separations (10 μm) correspond with the nanotube length (2.4−3.5 μm). These observations suggest that cellular separation is not the key factor that dictates either the nanotube formation or the nanotube length, but the local presentation of haptens is important to the formation. These comparisons also partly explain the observed low prevalence of the membrane nanotube formation; for example, the geometry of hapten in Nano2 facilitates nanotube formation for individual cells, but the intercellular separation may be too far for all populations to bridge.

Possible Mechanism of the Nanostructure-Induced Formation of Membrane Nanotubes among RBL Cells. Important and pertinent information is summarized below to rationalize the formation of membrane nanotubes among RBL cells. Prior work indicated that the formation of cytoneme-like nanotubes among BMMCs occurred 5 min after co-stimulation of FcεRI and CCR1, by DNP-HSA and MIP-1α, respectively.[33] Due to lack of CCR1 receptors at cell membranes, it was found unlikely to induce cytoneme-like nanotubes among RBL cells. Cytoneme-like nanotube formation was attributed to CCR1 activation and Ca^{2+} accumulation, with a possible origin of hydrostatic pressure to drive pseudopod extensions of internal membranes.[33]

FcεRI at the cellular membrane are known to mediate various signaling cascades among mast cells, such as antigen-induced degranulation,[18,40,41] cytokine production,[41] eicosanoid production,[19] phagocytosis, and cell migration and adhesion.[40] The most well-known signaling pathway is the IgE-specific antigen induced degranulation.[15,17] Soluble multivalent antigens were utilized to induce activation with high efficacy, because these ligands cross-link FcεRI and trigger downstream signaling pathways leading to degranulation.[17,18,42,43] Our prior work revealed that surface-bound antigens, when positioned at a matching geometry of closely packed FcεRI protein molecules, exhibit high potency in activating mast cells.[16] This evidence, collectively, suggests that the presentation of the antigen or hapten at the nanometer level dictates the arrangement of cellular receptors and thus impacts signaling pathways. Specifically, clustering (in 20 nm periodicity) of antigen such as DNP hepten is known to activate antibody-FcεRI-mediated activation among mast cells, while lack of or significant reduction of clustering hampers the activation signaling cascades.

As illustrated in Figure 6A and B, upon presenting DNP on a nanogrid, FcεRI proteins cluster into an almost 2D close-packed fashion.[16] This spatial arrangement brings FcεRI and Lyn into proximity. Lyn plays a positive role in this signaling pathway,[40] leading to phosphorylation of tyrosine residues within ITAMs in FcεRI.[16,17,20] Phosphorylated ITAMs then serve as docking sites for Syk.[20,40] The binding of Syk results in activation of Syk and leads to downstream signaling pathways resulting in degranulation and F-actin reorganization.[18,20,40] The membrane ridges are characteristic of this antigen-induced activation of mast cells.[41,44]

In the design of Nano1−Nano6, we purposefully deviate from the 20 nm hexagonal arrangement. Instead, our nanorings allow FcεRI dimers to form, but the separation among dimers is significantly larger than 20 nm, therefore discouraging the formation of

TABLE 2. Presentation of DNP Hapten at the Nanometer Level in Correlation with Membrane Nanotube Formation Efficacy

DNP presentation	local strucutures of DNP (nm)	DNP coverage (%)	nanotube length (μm)	nanotube prevalence (%)
Nano1	nanoring periodicity 1001 ± 11	15 ± 1	5.0—11.2	11 ± 2
Nano2	nanoring periodicity 807 ± 10	20 ± 1	4.6—12.7	12 ± 3
Nano3	nanoring periodicity 507 ± 9	34 ± 2	3.7—8.2	10 ± 3
Nano4	nanoring periodicity 305 ± 7	51 ± 3	3.5—7.9	9 ± 3
Nano5	nanoring periodicity 241 ± 6	62 ± 5	3.2—7.6	5 ± 2
Nano6	nanoring periodicity 207 ± 6	72 ± 6	2.4—3.5	0—3
SAM1	domain size 8—28 separation 46 ± 10	22.6	N/A	0
SAM2	domain size 7—24 separation 24 ± 9	34.1	5.2	0—0.2
SAM3	strips width 17—65 separation 10—33	89.5	4.3—6.6	0—0.5

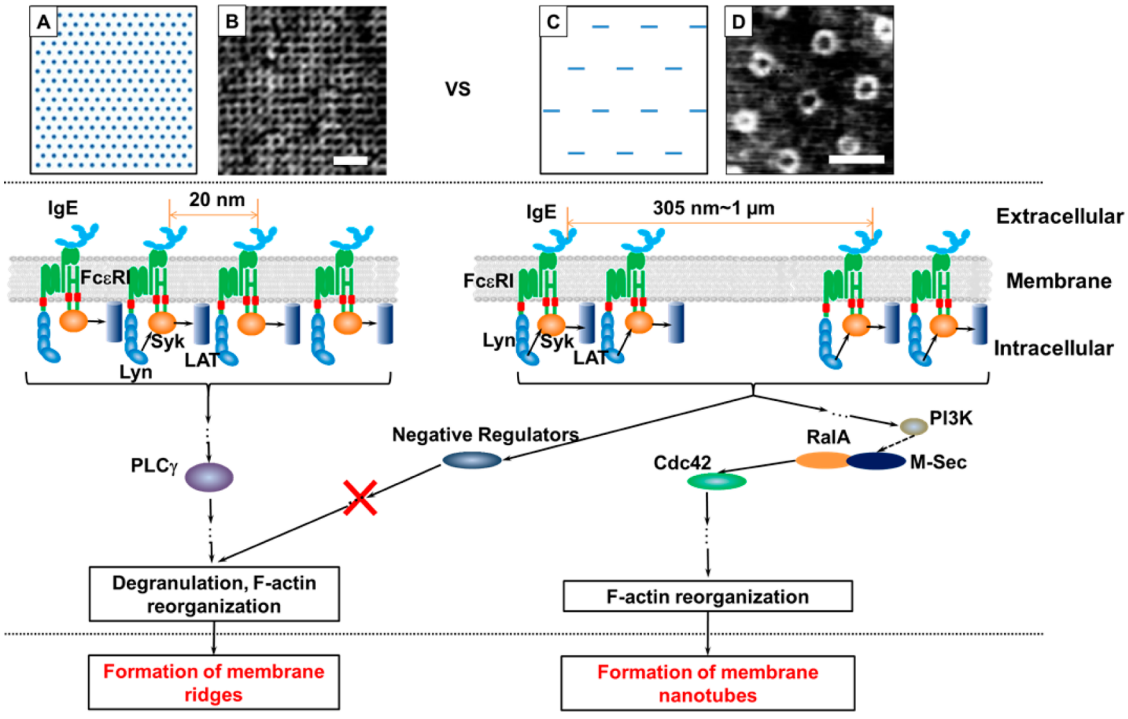

Figure 6. Schematic diagram to illustrate DNP nanostructure-induced signaling processes among RBL cells. (A) From the perspective of geometry only, the optimal arrangement of IgE-FcεRI complexes for degranulation. (B) AFM topographic image of DNP nanostructures produced using nanografting.[45−53] The periodicity of this DNP grid nanostructure is 39 ± 4 nm, and the edge-to-edge separation is 22 ± 5 nm.[16] (C) From the perspective of geometry only, arrangements of IgE-FcεRI complexes for discouraging degranulation and facilitating nanotube formation. (D) AFM topographic image of Nano2. Scale bars are as follows: (B) 100 nm; (D) 800 nm.

2D clusters. From SEM images shown in Figures 2, 3, 4, and 7F, few ridges were observed among RBL cells bridged by membrane nanotubes. Only microvilli are visible, as seen in Figure 7F. In contrast, membrane ridges are clearly observed on activated RBL by pure DNP SAMs, as shown in Figure 7E.

Therefore, under this design guide as shown in Figure 6C and D, the hapten arrangements enable binding with FcεRI proteins, which in turn recruit Lyn. Since this arrangement significantly deviates from the optimal arrangement (20 nm closely packed clustering), Lyn could have a negative regulation effect on

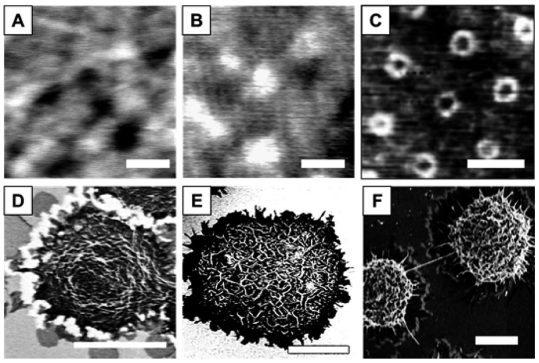

Figure 7. AFM topography images of (A) SAM1, (B) pure DNP SAMs, and (C) Nano2. SEM images of RBL cells after a 1 h interaction with (D) SAM1, (E) pure DNP SAMs, and (F) Nano2. Scale bars are as follows: (A, B) 25 nm; (C) 800 nm; (D−F) 10 μm.

degranulation cascades[54−58] through various negative regulators, such as SHIP and SHP.[40,58] Lyn-mediated negative regulation is consistent with our observations that at least one of the two mast cells when bridging does not exhibit membrane ridges, a characteristic structure for degranulation. In the meantime, the spatial arrangement supports downstream activation of PI3K, which is a key factor in regulating F-actin reorganization in mast cells.[59] On the basis of previous investigations,[60,61] activated PI3K may trigger M-Sec-mediated membrane nanotube formation. To completely unveil the optimal arrangement and signaling pathways, a systematic knockout of the signaling proteins needs to be performed.

To further reveal the significance of the spatial arrangement of hapten, a mixed DNP/C18 SAM (SAM1) with the same DNP coverage as Nano2 was used, as shown in Figure 7A. After 1 h interaction with SAM1, as shown in Figure 7D, one could observe hardly any membrane nanotubes. Similarly, two other SAMs, SAM2 and SAM3, with similar DNP coverage to Nano3 and Nano6, respectively, were tested. Near zero prevalence was observed. The measurements are also summarized in Table 2 and Figure 5. In all SAMs tested, there were no periodic arrangements of DNP domains, in contrast to the four nanostructures. The local presentations of DNP in SAMs are defined by the DNP domains (full width at half-maximum, FWHF, in topographs) separated by defects or alkanethiol areas.[62−66] Separations are quantified from AFM topographic images. While the DNP domains in SAMs are sufficiently large to enable FcεRI dimer formation, the interdomain distance varies; as such, the presentation does not facilitate large 2D receptor clusters or maintain sparse separations.

CONCLUSIONS

Using RBL cells as a mast cell model, this work reports an important finding; membrane nanotubes can form upon interaction with hapten nanostructures. This finding was a surprise at first glance, because RBL should not form membrane nanotubes by simple FcεRI stimulation, due to the lack of CCR1 on the cell surface. Formation of membrane nanotubes among BMMCs is known by co-stimulation of FcεRI and CCR1 *via* antigen and MIP-1α, respectively. Our study demonstrates that a key factor for selective activation of a cellular signaling cascade is the local presentation of ligands, in this case, hapten. The arrays of DNP nanorings with hundreds of nanometer separation discourage the clustering of FcεRI receptors, which therefore hampers the antigen-induced degranulation. As such, RBL cells rearrange their cytoskeleton structure to form nanotubes following this stimulation. These results demonstrate an important scientific concept; nanotechnology offers a new platform to selectively activate desired cellular signaling cascades. This finding is of general importance, and we envision more practice of this approach utilizing other ligand−receptor interactions and their corresponding cellular signaling processes, such as regulation of cancer cell proliferation and migration, stem cell differentiation, and impacting tissue engineering.

METHODS

Reagents. Reagents were used without further purification unless described specifically. Organosilanes, including *N*-(6-aminohexyl)aminopropyltrimethoxysilane (AAPTMS) and octadecyltrichlorosilane (OTS), were purchased from Gelest (Morrisville, PA, USA). Polystyrene microspheres were purchased from Thermo Scientific (Waltham, MA, USA). The spheres were suspended in their original concentration of 2% (w/v, aqueous) until usage. Polished silicon wafers, Si(111) doped with boron, were purchased from Virginia Semiconductor Inc. (Fredericksburg, VA, USA). Gold slugs (99.999%) were purchased from Alfa Aesar (Ward Hill, MA, USA). Hapten molecules, $[DNPNH(CH_2)_5COO(CH_2CH_2O)_4CO(CH_2)_{15}S]_2$ (DNP-thiol), with a purity of >95% were purchased from ProChimia (Gdansk, Poland). 2-Butanol was purchased from Fisher Scientific (Pittsburgh, PA, USA), and ethanol (EtOH, 99.99%) was purchased from Gold Shield Chemical Co. (Hayward, CA, USA). Sulfuric acid (95.0%), hydrogen peroxide (30% aqueous solution), ammonium hydroxide (30% aqueous solution), and *N*,*N*-dimethylformamide (DMF) were purchased from EMD Chemicals (Gibbstown, NJ, USA). Fetal bovine serum (FBS), Dulbecco's modified Eagle medium (DMEM), and penicillin/streptomycin were purchased from Gibco by Life Technologies (Grand Island, NY, USA). HEPES buffer solution (1 M) and phosphate-buffered saline (PBS) (1×) were purchased from Cellgro by Mediatech Inc. (Herndon, VA, USA). High-quality monoclonal mouse-anti-DNP IgE was attained following protocols developed by our team, previously.[67] Nitrogen gas (99.999%) and hydrogen gas (99.95%) were purchased from Praxair, Inc. (Danbury, CT, USA). Octadecanethiol (C18SH), *N*-succinimidyl *N*-(2,4-dinitrophenyl)-6-aminocaproate (DNP-NHS ester), dimethyl sulfoxide (DMSO), 37% formaldehyde solution, 25% glutaraldehyde solution, 4% osmium tetroxide (OsO_4) solution, and hexamethyldisilazane (HMDS) were purchased from Sigma-Aldrich (St. Louis, MO, USA). Toluene and 2-butanol were purchased from Fisher Scientific (Pittsburgh, PA, USA).

Rat basophilic leukemia cells (RBL-2H3) were purchased from ATCC (Manassas, VA, USA). Deionized and ultrapure water was attained from a Milli-Q water system (EMD Millipore, Billerica, MA, USA). Mica sheets (clear ruby muscovite) were purchased from Mica New York Corp.

Preparation of Hapten Nanostructures on Silicon Substrates. Particle lithography followed by vapor deposition was used to produce AAPTMS nanopatterns on silicon surfaces, following previously reported protocols.[68−71] Polished silicon wafers were cleaned by immersion in piranha solution for 1 h and subsequently in basic solution at 70 °C for 1 h. Piranha solution was prepared by mixing sulfuric acid and hydrogen peroxide at a volume ratio of 3:1. It is highly corrosive and should be handled carefully. Basic bath was prepared by mixing NH_4OH, H_2O_2 solution, and H_2O at a volume ratio of 1:1:5. Wafers were then rinsed copiously with water and dried in N_2. Polystyrene microspheres were washed, then separated from solvent by centrifugation to remove additives such as charge stabilizers or surfactants. After cleaning, polystyrene microspheres were resuspended in aqueous solutions by sonication and used immediately afterward. A drop (20 μL) of the microsphere solution was deposited on the clean Si(111) surfaces and allowed to spread and dry to produce a mask of closely packed microspheres. Next, the wafer was placed into a sealed Teflon container (100 mL) containing 200 μL of AAPTMS, then heated in an oven at 70−80 °C for 6 h. During heating, AAPTMS molecules from vapor attached to uncovered interstitial areas. The polystyrene microsphere masks were removed by a 10 min sonication in both ethanol and deionized water, sequentially.

The AAPTMS nanopatterns formed were immersed in 1 mM OTS solution (toluene based) for 4 h, in order to fill the void on the Si surfaces. Afterward, the samples were cleaned by sonication in ethanol for 15 min. The DNP functionalization was achieved by cross-linking the DNP-NHS ester (1 mg/mL in 1 M HEPES buffer) to primary amine termini of the AAPTMS nanopatterns. The reaction took 12 h to complete at room temperature. Finally, these DNP nanostructures were rinsed with DMSO, then ethanol, to remove nonreacted residues and then dried with N_2.

Preparation of Self-Assembled Monolayers on Gold Thin Films. Gold thin films on mica were produced following previous protocols.[72−76] Briefly, gold was deposited onto freshly cleaved mica surfaces in a high-vacuum evaporator (model DV502-A, Denton Vacuum, Moorestown, NJ, USA) at a base pressure below 2×10^{-6} Torr. The typical evaporation rates were 3 Å/s, and the thickness of the gold films was controlled at 150 nm. Immediately after removal from the vacuum chamber, the mica-supported gold films were subject to H_2 flaming to remove combustible contaminants and to improve Au(111) terrace size. The thin gold film on mica was cooled in air to room temperature and kept for the fabrication of SAMs.

Two pure component SAMs, C18SH SAMs, DNP-terminated SAMs, and three binary SAMs consisting of C18SH and DNP-thiol at designated compositions were prepared on Au(111) surfaces following previously reported protocols.[16] C18SH SAMs were typically prepared by immersing mica-supported gold films in a 0.02 mM C18SH solution in 2-butanol for 24 h. DNP-terminated SAMs followed a similar protocol, except the solvent was a mixture of DMF/2-butanol (1:19). The three binary SAMs were prepared similarly, except for the thiol solutions, mixing DNP-thiol and C18SH stock solutions to reach designated molar ratios of 1:20, 1:1, and 20:1, referred to as SAM1, SAM2, and SAM 3, respectively.

AFM Characterization. An atomic force microscope (MFP-3D, Asylum Research Corp., Santa Barbara, CA, USA) was used for the structural characterization of DNP nanostructures, SAMs, and cells. All AFM images were acquired under contact mode with imaging forces of 15−25 nN. Silicon cantilevers with a spring constant of 0.1 N/m were purchased from Bruker (MSNL, Camarillo, CA, USA). The AFM images were acquired and analyzed using Asylum MFP3D software developed on the Igor Pro 6.12 platform.

Calculation of DNP Coverage of Nanostructures. The DNP coverage of each nanostructure is calculated by the following formula:

$$\text{DNP coverage} = \frac{\pi W^2 + \pi DW}{a^2 \sin 60°}$$

where W represents ring width, D represents inner diameter, and a represents periodicity for each nanostructure.

Culture of RBL-2H3 Cells. RBL-2H3 cells were thawed by gentle agitation in a 37 °C water bath upon receipt. RBL cells were then maintained at 37 °C and 5% CO_2 in DMEM cell medium containing 20% FBS and 1% penicillin/streptomycin, following established protocols.[15] Cells were first sensitized with 0.5 μg/mL anti-DNP IgE overnight and then washed with PBS to remove excess IgE. The sensitized RBL-2H3 cells were then utilized to study membrane nanotube formation upon contacting designated surfaces such as hapten nanostructures and/or SAMs mentioned.

SEM Imaging of RBL-2H3 Cells. Sample preparation for SEM characterization followed known protocols.[16] Briefly, a 1:1 mixture of 25% glutaraldehyde and 37% formaldehyde was diluted 10-fold with deionized water and used as a primary fixative. The silicon wafers containing RBL cells were taken out from the culture medium and rinsed with PBS. Then, the wafers were immersed in primary fixative for 1 h. The 4% OsO_4 solution was diluted with deionized water into a 1% solution for sample preparation. After 1 h immersion in primary fixative, the samples were rinsed with deionized water three times followed by soaking in 1% OsO_4 solution for 30 min. Cell samples were then subjected to a sequential 10 min immersion−removal of ethanol/water mixtures with an increasing ethanol content of 25, 50, 75, 90, and 100%, respectively. The final step of dehydration in pure ethanol was repeated three times, followed by addition of HMDS, the drying agent for biological samples as previously reported.[77−79] The surface-support cells were then mounted to the SEM sample holder and transported to the vacuum chamber. The morphology of RBL-2H3 cells was imaged with a Hitachi S-4100T FE-SEM (Hitachi High Technologies America, Inc., Pleasanton, CA, USA), under an accelerating voltage of 2 kV at 10 μA.

Conflict of Interest: The authors declare no competing financial interest.

Acknowledgment. We would like to thank Mr. Alan Hicklin at the UC Davis' Keck Spectral Imaging Facility for his technical assistance, and Ms. Susan Stagner for her help in the preparation of the manuscript. This work was supported by National Institutes of Health (1R21CA176850-01) and the Gordon and Betty Moore Foundation. S.S.R. is a recipient of the Alfred P. Sloan Foundation Minority Ph.D. Scholarship. Y.L. is supported by a UCD-LLNL Joint Graduate Mentorship Award.

REFERENCES AND NOTES

1. Sherer, N. M.; Mothes, W. Cytonemes and Tunneling Nanotubules in Cell-Cell Communication and Viral Pathogenesis. *Trends Cell Biol.* **2008**, *18*, 414–420.
2. Gerdes, H.-H.; Bukoreshtliev, N. V.; Barroso, J. F. V. Tunneling Nanotubes: A New Route for the Exchange of Components between Animal Cells. *FEBS Lett.* **2007**, *581*, 2194–2201.
3. Onfelt, B.; Nedvetzki, S.; Yanagi, K.; Davis, D. M. Cutting Edge: Membrane Nanotubes Connect Immune Cells. *J. Immunol.* **2004**, *173*, 1511–1513.
4. Watkins, S. C.; Salter, R. D. Functional Connectivity between Immune Cells Mediated by Tunneling Nanotubules. *Immunity* **2005**, *23*, 309–318.
5. Antanavičiūtė, I.; Rysevaitė, K.; Liutkevičius, V.; Marandykina, A.; Rimkutė, L.; Sveikatienė, R.; Uloza, V.; Skeberdis, V. A. Long-Distance Communication between Laryngeal Carcinoma Cells. *PLoS One* **2014**, *9*, e99196.
6. Ratajczak, M. Z.; Kucia, M.; Dobrowolska, H.; Wanzeck, J.; Reca, R.; Ratajczak, J. Emerging Concept of Cancer as a Stem Cell Disorder. *Cent. Eur. J. Biol.* **2006**, *1*, 73–87.
7. Bjerkvig, R.; Tysnes, B. B.; Aboody, K. S.; Najbauer, J.; Terzis, A. J. A. Opinion - The Origin of The Cancer Stem Cell: Current Controversies and New Insights. *Nat. Rev. Cancer* **2005**, *5*, 899–904.
8. Gousset, K.; Schiff, E.; Langevin, C.; Marijanovic, Z.; Caputo, A.; Browman, D. T.; Chenouard, N.; de Chaumont, F.; Martino, A.; Enninga, J.; *et al.* Prions Hijack Tunnelling

Nanotubes for Intercellular Spread. *Nat. Cell Biol.* **2009**, *11*, 328–336.
9. Sowinski, S.; Jolly, C.; Berninghausen, O.; Purbhoo, M. A.; Chauveau, A.; Köhler, K.; Oddos, S.; Eissmann, P.; Brodsky, F. M.; Hopkins, C.; *et al*. Membrane Nanotubes Physically Connect T Cells over Long Distances Presenting a Novel Route for HIV-1 Transmission. *Nat. Cell Biol.* **2008**, *10*, 211–219.
10. Koyanagi, M.; Brandes, R. P.; Haendeler, J.; Zeiher, A. M.; Dimmeler, S. Cell-to-Cell Connection of Endothelial Progenitor Cells with Cardiac Myocytes by Nanotubes - A Novel Mechanism for Cell Fate Changes? *Circ. Res.* **2005**, *96*, 1039–1041.
11. Kajstura, J.; Leri, A.; Bolli, R.; Anversa, P. Endothelial Progenitor Cells: Neovascularization or More? *J. Mol. Cell. Cardiol.* **2006**, *40*, 1–8.
12. Rustom, A.; Saffrich, R.; Markovic, I.; Walther, P.; Gerdes, H.-H. Nanotubular Highways for Intercellular Organelle Transport. *Science* **2004**, *303*, 1007–1010.
13. Davis, D. M.; Sowinski, S. Membrane Nanotubes: Dynamic Long-Distance Connections between Animal Cells. *Nat. Rev. Mol. Cell Biol.* **2008**, *9*, 431–436.
14. Onfelt, B.; Nedvetzki, S.; Benninger, R. K. P.; Purbhoo, M. A.; Sowinski, S.; Hume, A. N.; Seabra, M. C.; Neil, M. A. A.; French, P. M. W.; Davis, D. M. Structurally Distinct Membrane Nanotubes between Human Macrophages Support Long-Distance Vesicular Traffic or Surfing of Bacteria. *J. Immunol.* **2006**, *177*, 8476–8483.
15. Zuberi, R. I.; Frigeri, L. G.; Liu, F. T. Activation of Rat Basophilic Leukemia Cells by Epsilon-BP, an Ige-Binding Endogenous Lectin. *Cell. Immunol.* **1994**, *156*, 1–12.
16. Deng, Z.; Weng, I. C.; Li, J. R.; Chen, H. Y.; Liu, F. T.; Liu, G. Y. Engineered Nanostructures of Antigen Provide an Effective Means for Regulating Mast Cell Activation. *ACS Nano* **2011**, *5*, 8672–8683.
17. Sharma, B. B.; Apgar, J. R.; Liu, F. T. Mast Cells - Receptors, Secretagogues, and Signaling. *Clin. Rev. Allergy Immunol.* **2002**, *22*, 119–148.
18. Metcalfe, D. D.; Baram, D.; Mekori, Y. A. Mast Cells. *Physiol. Rev.* **1997**, *77*, 1033–1079.
19. Rivera, J.; Fierro, N. A.; Olivera, A.; Suzuki, R. New Insights on Mast Cell Activation via the High Affinity Receptor for IgE. *Adv. Immunol.* **2008**, *98*, 85–120.
20. Siraganian, R. P.; de Castro, R. O.; Barbu, E. A.; Zhang, J. Mast Cell Signaling: The Role of Protein Tyrosine Kinase Syk, Its Activation and Screening Methods for New Pathway Participants. *FEBS Lett.* **2010**, *584*, 4933–4940.
21. Otsuka, A.; Kabashima, K. Mast Cells and Basophils in Cutaneous Immune Responses. *Allergy* **2015**, *70*, 131–140.
22. Soucie, E.; Brenet, F.; Dubreuil, P. Molecular Basis of Mast Cell Disease. *Mol. Immunol.* **2015**, *63*, 55–60.
23. Sibilano, R.; Pucillo, C. E.; Gri, G. Allergic Responses and Aryl Hydrocarbon Receptor Novel Pathway of Mast Cell Activation. *Mol. Immunol.* **2015**, *63*, 69–73.
24. Merluzzi, S.; Betto, E.; Ceccaroni, A. A.; Magris, R.; Giunta, M.; Mion, F. Mast Cells, Basophils and B Cell Connection Network. *Mol. Immunol.* **2015**, *63*, 94–103.
25. da Silva, E. Z. M.; Jamur, M. C.; Oliver, C. Mast Cell Function: A New Vision of an Old Cell. *J. Histochem. Cytochem.* **2014**, *62*, 698–738.
26. Torres, A. J.; Wu, M.; Holowka, D.; Baird, B. Nanobiotechnology and Cell Biology: Micro- and Nanofabricated Surfaces to Investigate Receptor-Mediated Signaling. *Annu. Rev. Biophys.* **2008**, *37*, 265–288.
27. Torres, A. J.; Vasudevan, L.; Holowka, D.; Baird, B. A. Focal Adhesion Proteins Connect IgE Receptors to the Cytoskeleton as Revealed by Micropatterned Ligand Arrays. *Proc. Natl. Acad. Sci. U.S.A.* **2008**, *105*, 17238–17244.
28. Orth, R. N.; Wu, M.; Holowka, D. A.; Craighead, H. G.; Baird, B. A. Mast Cell Activation on Patterned Lipid Bilayers of Subcellular Dimensions. *Langmuir* **2003**, *19*, 1599–1605.
29. Holowka, D.; Sil, D.; Torigoe, C.; Baird, B. Insights into Immunoglobulin E Receptor Signaling from Structurally Defined Ligands. *Immunol. Rev.* **2007**, *217*, 269–279.
30. Henz, B. M.; Maurer, M.; Lippert, U.; Worm, M.; Babina, M. Mast Cells as Initiators of Immunity and Host Defense. *Exp. Dermatol.* **2001**, *10*, 1–10.
31. Taylor, M. L.; Metcalfe, D. D. Mast Cells in Allergy and Host Defense. *Allergy Asthma Proc.* **2001**, *22*, 115–119.
32. Pulendran, B.; Ono, S. J. A Shot in the Arm for Mast Cells. *Nat. Med.* **2008**, *14*, 489–490.
33. Fifadara, N. H.; Beer, F.; Ono, S.; Ono, S. J. Interaction between Activated Chemokine Receptor 1 and Fc Epsilon RI at Membrane Rafts Promotes Communication and F-Actin-Rich Cytoneme Extensions between Mast Cells. *Int. Immunol.* **2010**, *22*, 113–128.
34. Wang, Z. G.; Liu, S. L.; Tian, Z. Q.; Zhang, Z. L.; Tang, H. W.; Pang, D. W. Myosin-Driven Intercellular Transportation of Wheat Germ Agglutinin Mediated by Membrane Nanotubes between Human Lung Cancer Cells. *ACS Nano* **2012**, *6*, 10033–10041.
35. He, K.; Luo, W.; Zhang, Y.; Liu, F.; Liu, D.; Xu, L.; Qin, L.; Xiong, C.; Lu, Z.; Fang, X.; Zhang, Y. Intercellular Transportation of Quantum Dots Mediated by Membrane Nanotubes. *ACS Nano* **2010**, *4*, 3015–3022.
36. Lizana, L.; Konkoli, Z.; Bauer, B.; Jesorka, A.; Orwar, O. Controlling Chemistry by Geometry in Nanoscale Systems. *Annu. Rev. Phys. Chem.* **2009**, *60*, 449–468.
37. Rainy, N.; Chetrit, D.; Rouger, V.; Vernitsky, H.; Rechavi, O.; Marguet, D.; Goldstein, I.; Ehrlich, M.; Kloog, Y. H-Ras Transfers from B to T Cells via Tunneling Nanotubes. *Cell Death Dis.* **2013**, *4*, e726.
38. Rechavi, O.; Goldstein, I.; Vernitsky, H.; Rotblat, B.; Kloog, Y. Intercellular Transfer of Oncogenic H-Ras at the Immunological Synapse. *PLoS One* **2007**, *2*, e1204.
39. Rechavi, O.; Goldstein, I.; Kloog, Y. Intercellular Exchange of Proteins: The Immune Cell Habit of Sharing. *FEBS Lett.* **2009**, *583*, 1792–1799.
40. Gilfillan, A. M.; Rivera, J. The Tyrosine Kinase Network Regulating Mast Cell Activation. *Immunol. Rev.* **2009**, *228*, 149–169.
41. Rivera, J.; Gilfillan, A. M. Molecular Regulation of Mast Cell Activation. *J. Allergy Clin. Immunol.* **2006**, *117*, 1214–1225.
42. Wilson, B. S.; Pfeiffer, J. R.; Oliver, J. M. Fc Epsilon RI Signaling Observed from the inside of the Mast Cell Membrane. *Mol. Immunol.* **2002**, *38*, 1259–1268.
43. Gilfillan, A. M.; Tkaczyk, C. Integrated Signalling Pathways for Mast-Cell Activation. *Nat. Rev. Immunol.* **2006**, *6*, 218–230.
44. Pfeiffer, J. R.; Seagrave, J. C.; Davis, B. H.; Deanin, G. G.; Oliver, J. M. Membrane and Cytoskeletal Changes Associated with IgE-Mediated Serotonin Release from Rat Basophilic Leukemia Cells. *J. Cell Biol.* **1985**, *101*, 2145–2155.
45. Headrick, J. E.; Armstrong, M.; Cratty, J.; Hammond, S.; Sheriff, B. A.; Berrie, C. L. Nanoscale Patterning of Alkyl Monolayers on Silicon Using the Atomic Force Microscope. *Langmuir* **2005**, *21*, 4117–4122.
46. Marchin, K. L.; Berrie, C. L. Conformational Changes in the Plasma Protein Fibrinogen upon Adsorption to Graphite and Mica Investigated by Atomic Force Microscopy. *Langmuir* **2003**, *19*, 9883–9888.
47. Toriyama, M.; Maher, T. R.; Holovics, T. C.; Vanka, K.; Day, V. W.; Berrie, C. L.; Thompson, W. H.; Barybin, M. V. Multipoint Anchoring of the [2.2.2.2]Metacyclophane Motif to a Gold Surface via Self-Assembly: Coordination Chemistry of a Cyclic Tetraisocyanide Revisited. *Inorg. Chem.* **2008**, *47*, 3284–3291.
48. Headrick, J. E.; Berrie, C. L. Alternative Method for Fabricating Chemically Functionalized AFM Tips: Silane Modification of HF-Treated Si_3N_4 Probes. *Langmuir* **2004**, *20*, 4124–4131.
49. Bano, F.; Fruk, L.; Sanavio, B.; Glettenberg, M.; Casalls, L.; Niemeyer, C. M.; Scoles, G. Toward Multiprotein Nanoarrays Using Nanografting and DNA Directed Immobilization of Proteins. *Nano Lett.* **2009**, *9*, 2614–2618.
50. Camillone, N.; Leung, T. Y. B.; Schwartz, P.; Eisenberger, P.; Scoles, G. Chain Length Dependence of the Striped Phases of Alkanethiol Monolayers Self-Assembled on

Au(111): An Atomic Beam Diffraction Study. *Langmuir* **1996**, *12*, 2737–2746.
51. Staii, C.; Wood, D. W.; Scoles, G. Ligand-Induced Structural Changes in Maltose Binding Proteins Measured by Atomic Force Microscopy. *Nano Lett.* **2008**, *8*, 2503–2509.
52. Tian, T.; LeJeune, Z. M.; Serem, W. K.; Yu, J. J.; Garno, J. C. In *Tip-Based Nanofabrication: Fundamentals and Applications*; Tseng, A. A., Ed.; Springer: New York, 2011; pp 167–205.
53. Garno, J. C.; Batteas, J. D. In *Applied Scanning Probe Methods IV: Industrial Applications*; Bhushan, B., Fuchs, H., Eds.; Springer: New York, 2006; pp 105–135.
54. Odom, S.; Gomez, G.; Kovarova, M.; Furumoto, Y.; Ryan, J. J.; Wright, H. V.; Gonzalez-Espinosa, C.; Hibbs, M. L.; Harder, K. W.; Rivera, J. Negative Regulation of Immunoglobulin E-Dependent Allergic Responses by Lyn Kinase. *J. Exp. Med.* **2004**, *199*, 1491–1502.
55. Hernandez-Hansen, V.; Smith, A. J.; Surviladze, Z.; Chigaev, A.; Mazel, T.; Kalesnikoff, J.; Lowell, C. A.; Krystal, G.; Sklar, L. A.; Wilson, B. S.; *et al*. Dysregulated Fc Epsilon RI Signaling and Altered Fyn And Ship Activities in Lyn-Deficient Mast Cells. *J. Immunol.* **2004**, *173*, 100–112.
56. Xiao, W. B.; Nishimoto, H.; Hong, H.; Kitaura, J.; Nunomura, S.; Maeda-Yamamoto, M.; Kawakami, Y.; Lowell, C. A.; Ra, C. S.; Kawakami, T. Positive and Negative Regulation of Mast Cell Activation by Lyn via The Fc Epsilon RI. *J. Immunol.* **2005**, *175*, 6885–6892.
57. Huber, M.; Helgason, C. D.; Damen, J. E.; Liu, L.; Humphries, R. K.; Krystal, G. The Src Homology 2-Containing Inositol Phosphatase (SHIP) is the Gatekeeper of Mast Cell Degranulation. *Proc. Natl. Acad. Sci. U.S.A.* **1998**, *95*, 11330–11335.
58. Leung, W. H.; Bolland, S. The Inositol 5′-Phosphatase SHIP-2 Negatively Regulates IgE-Induced Mast Cell Degranulation and Cytokine Production. *J. Immunol.* **2007**, *179*, 95–102.
59. Draber, P.; Sulimenko, V.; Draberova, E. Cytoskeleton in Mast Cell Signaling. *Front. Immunol.* **2012**, *3*, 130–130.
60. Hase, K.; Kimura, S.; Takatsu, H.; Ohmae, M.; Kawano, S.; Kitamura, H.; Ito, M.; Watarai, H.; Hazelett, C. C.; Yeaman, C.; *et al*. M-Sec Promotes Membrane Nanotube Formation by Interacting with Ral and the Exocyst Complex. *Nat. Cell Biol.* **2009**, *11*, 1427–U91.
61. Wang, Y.; Cui, J.; Sun, X.; Zhang, Y. Tunneling-Nanotube Development in Astrocytes Depends on p53 Activation. *Cell Death Differ.* **2011**, *18*, 732–742.
62. Kumar, A.; Abbott, N. L.; Biebuyck, H. A.; Kim, E.; Whitesides, G. M. Patterned Self-Assembled Monolayers and Meso-Scale Phenomena. *Acc. Chem. Res.* **1995**, *28*, 219–226.
63. Xia, Y.; Whitesides, G. M. Use of Controlled Reactive Spreading of Liquid Alkanethiol on the Surface of Gold to Modify the Size of Features Produced by Microcontact Printing. *J. Am. Chem. Soc.* **1995**, *117*, 3274–3275.
64. Dubois, L. H.; Nuzzo, R. G. Synthesis, Structure, and Properties of Model Organic Surfaces. *Annu. Rev. Phys. Chem.* **1992**, *43*, 437–463.
65. Nuzzo, R. G.; Allara, D. L. Adsorption of Bifunctional Organic Disulfides on Gold Surfaces. *J. Am. Chem. Soc.* **1983**, *105*, 4481–4483.
66. Bain, C. D.; Troughton, E. B.; Tao, Y. T.; Evall, J.; Whitesides, G. M.; Nuzzo, R. G. Formation of Monolayer Films by the Spontaneous Assembly of Organic Thiols from Solution onto Gold. *J. Am. Chem. Soc.* **1989**, *111*, 321–335.
67. Liu, F. T.; Bohn, J. W.; Ferry, E. L.; Yamamoto, H.; Molinaro, C. A.; Sherman, L. A.; Klinman, N. R.; Katz, D. H. Monoclonal Dinitrophenyl-Specific Murine Ige Antibody - Preparation, Isolation, and Characterization. *J. Immunol.* **1980**, *124*, 2728–2737.
68. Li, J. R.; Lusker, K. L.; Yu, J. J.; Garno, J. C. Engineering the Spatial Selectivity of Surfaces at the Nanoscale Using Particle Lithography Combined with Vapor Deposition of Organosilanes. *ACS Nano* **2009**, *3*, 2023–2035.
69. Li, J. R.; Garno, J. C. Elucidating the Role of Surface Hydrolysis in Preparing Organosilane Nanostructures via Particle Lithography. *Nano Lett.* **2008**, *8*, 1916–1922.
70. Lin, W. F.; Swartz, L. A.; Li, J. R.; Liu, Y.; Liu, G. Y. Particle Lithography Enables Fabrication of Multicomponent Nanostructures. *J. Phys. Chem. C* **2013**, *117*, 23279–23285.
71. Lin, W. F.; Li, J. R.; Liu, G. Y. Near-Field Scanning Optical Microscopy Enables Direct Observation of Moiré Effects at the Nanometer Scale. *ACS Nano* **2012**, *6*, 9141–9149.
72. Shi, L.; Fleming, C. J.; Riechers, S. L.; Yin, N. N.; Luo, J.; Lam, K. S.; Liu, G. Y. High-Resolution Imaging of Dendrimers Used in Drug Delivery via Scanning Probe Microscopy. *J. Drug Delivery* **2011**, *2011*, 254095–254095.
73. Li, J. R.; Yin, N. N.; Liu, G. Y. Hierarchical Micro- and Nanoscale Structures on Surfaces Produced Using a One-Step Pattern Transfer Process. *J. Phys. Chem. Lett.* **2011**, *2*, 289–294.
74. Kurniawan, J.; Yin, N. N.; Liu, G. Y.; Kuhl, T. L. Interaction Forces between Ternary Lipid Bilayers Containing Cholesterol. *Langmuir* **2014**, *30*, 4997–5004.
75. Yin, N. N.; Buyanin, A.; Riechers, S. L.; Lee, O. P.; Frechet, J. M. J.; Salmeron, M.; Liu, G. Y. In Situ and Real-Time Atomic Force Microscopy Studies of the Stability of Oligothiophene Langmuir-Blodgett Monolayers in Liquid. *J. Phys. Chem. C* **2014**, *118*, 5789–5795.
76. Fleming, C. J.; Yin, N. N.; Riechers, S. L.; Chu, G.; Liu, G. Y. High-Resolution Imaging of the Intramolecular Structure of Indomethacin-Carrying Dendrimers by Scanning Tunneling Microscopy. *ACS Nano* **2011**, *5*, 1685–1692.
77. Carr, J. H.; Anderson, R. L.; Favero, M. S. Comparison of Chemical Dehydration and Critical Point Drying for the Stabilization and Visualization of Aging Biofilm Present on Interior Surfaces of PVC Distribution Pipe. *J. Appl. Bacteriol.* **1996**, *80*, 225–232.
78. Braet, F.; deZanger, R.; Wisse, E. Drying Cells for SEM, AFM and TEM by Hexamethyldisilazane: A Study on Hepatic Endothelial Cells. *J. Microsc.-Oxford* **1997**, *186*, 84–87.
79. Araujo, J. C.; Teran, F. C.; Oliveira, R. A.; Nour, E. A. A.; Montenegro, M. A. P.; Campos, J. R.; Vazoller, R. F. Comparison of Hexamethyidisilazane and Critical Point Drying Treatments for SEM Analysis of Anaerobic Biofilms and Granular Sludge. *J. Electron Microsc.* **2003**, *52*, 429–433.